COMPUTATION AND CONTROL OF ASYMMETRIC VORTEX FLOW AROUND CIRCULAR CONES USING NAVIER-STOKES EQUATIONS

Osama A. Kandil*, Tin-Chee Wong and Hamdy A. Kandil****
Old Dominion University, Norfolk, VA, USA
C. H. Liu***
NASA Langley Research Center, Hampton, VA, USA

Abstract

The unsteady, compressible, thin-layer and full Navier-Stokes equations are used to numerically simulate steady and unsteady asymmetric, supersonic, locally-conical flows around a 5°–semiapex angle circular cone. The main computational scheme which is used in this paper is the implicit, upwind, flux-difference splitting, finite-volume scheme. Comparison of asymmetric flow solutions using the thin-layer and full Navier-Stokes equations is presented and discussed. The implicit, upwind, flux-vector splitting, finite-volume scheme has also been used to solve for the unsteady asymmetric flow with vortex shedding. The unsteady-flow solution using the flux-vector splitting scheme perfectly agrees with the previously obtained solution using the flux-difference splitting scheme. Passive control of asymmetric flows has been demonstrated and studied using sharp- and round-edged, thick and thin strakes.

Introduction

At cruise conditions, where the angle of attack is small, most flight vehicles are designed to operate with attached flows. In the moderate to high angle-of-attack (AOA) ranges, which are typical conditions for highly maneuvering fighter aircraft and missiles,extensive regions of large-scale vortices develop on the leeward sides of the vehicle highly swept wings and slender body. Within these AOA ranges, the cross-flow velocity components and the gradients of other flow variables become of the same order of magnitude or higher than those of the axial direction. Consequently, flow separation occur and vortices emanate from the three-dimensional separation lines of boundary-layer flows on wings, strakes and fuselage of the vehicle. If the vortices are symmetric and stable, their influence could be exploited favorably to provide high lift and maneuverability for the vehicle. On the other hand, if the vortices become asymmetric or if vortex breakdown occurs, the useful influence of the vortices is terminated. Large side forces, asymmetric lifting forces and corresponding yawing, rolling and pitching moments, which may be larger than those available by the vehicle control system, develop and jeopardize flight safety. The onset of buffeting due to vortex breakdown is another unfavorable vortex-induced phenomenon.

Highly swept, round and sharp-leading-edge wings and pointed slender bodies are common aerodynamic components to fighter aircraft and missiles. The study of vortex-dominated flow around these isolated aerodynamic components adds to our basic understanding of vortical flows under various conditions including unsteady vortex-dominated flows, vortex-shock interaction and asymmetric vortex flow breakdown. In this paper, we focus on the problem of asymmetric vortex flow about slender bodies in the high AOA range. The problem is of vital importance to the dynamic stability and controllability of missiles and fighter aircraft.

The onset of flow asymmetry occurs when the relative incidence (ratio of angle of attack to nose semi-apex angle) of pointed forebodies exceeds certain critical values. At these critical values of relative incidence, flow asymmetry develops due to natural and/or forced disturbances. The origin of natural disturbances may be a transient side slip, an acoustic disturbance, or likewise disturbance of short duration. The origin of forced disturbances is geometric perturbations due to imperfections in the nose geometric symmetry or likewise disturbances of permanent nature. In addition to the relative incidence as one of the determinable parameters for the onset of flow asymmetry, the freestream Mach number, Reynolds number and shape of the body-cross sectional area are important determinable parameters.

Kandil, Wong and Liu[1] used the unsteady, thin-layer Navier-Stokes equations along with two different implicit schemes to simulate asymmetric vortex flows around cones with different cross-section shapes. The numerical investigation was focused on a 5°–semiapex angle circular cone and local, conical flow was assumed. The first computational scheme was an implicit, upwind, flux-difference splitting, finite-volume scheme and the second one was an implicit, central-difference, finite-volume scheme. Keeping the Mach number and Reynolds number constants at 1.8 and 10^5, respectively, the angle of attack was varied from 10° to 30°. At α = 10°, a steady symmetric solution was obtained and the results of the two schemes were in excellent agreement. At α = 20° and irrespective of the type or level of the disturbance, a steady asymmetric solution was obtained and the results of the two schemes were in excellent agreement. Two types of flow disturbances were used; a random round-off error or a random truncation-error disturbance and a controlled transient side-slip disturbance with short duration. For the controlled transient side-slip disturbance, the solution was unique, and for the uncontrolled random disturbance, the solution was also unique with the exception of having the same asymmetry changing sides on the cone. At α = 30°, an unsteady asymmetric solution with vortex shedding was obtained, and the vortex shedding was perfectly periodic. Next, the angle of attack was kept fixed at 20° and the Mach number was

*Professor and Eminent Scholar, Department of Mechanical Engineering and Mechanics, Associate Fellow AIAA.
**Research Assistant, same Department, Member AIAA.
***Group Leader, Theoretical Flow Physics Branch, Senior member AIAA.

increased from 1.8 to 3.0 with a step of 0.4. The solutions showed that the asymmetry become weaker as the Mach number is increased. The flow recovered its symmetry when the Mach number reached 3.0. Selected solutions of steady and unsteady asymmetric flows have also been presented for cones with elliptic and diamond cross-sectional areas. Passive control of the flow asymmetry has been tentatively demonstrated by using a fin on the leeward side of the body along the plane of geometric symmetry.

Siclari[2] used the unsteady, Navier-Stokes equations with a multigrid, central-difference, finite-volume scheme to solve for steady asymmetric conical flows around cones with elliptic, diamond and biparabolic sections. He addressed steady-flow problems similar to those of the present authors in reference 1. He considered the flow around circular cones with semi-apex angles of 5°, 6°, 7° and 8° at an angle of attack of 20° and a Reynolds number of 10^5. Varying the Mach number from 1.4 to 3.0 with a step of 0.4, he showed that the flow recovered its symmetry as the Mach number increased. The higher the semi-apex angle was, the lower the Mach number was, for the flow to recover its symmetry. Fixing the Mach number at 1.8, the angle of attack at 20°, the Reynolds number at 10^5 and the semi-apex angle at 5°, he decreased the cross-section fineness ratio (ratio of width to length) for different cross-sectional shapes. He showed that the flow recovered its symmetry at a fineness ratio of 0.4 for the elliptic-section cone, at 0.6 for the biparabolic-section cone and at 0.6 for the diamond-section cone.

In a very recent paper by Kandil, Wong and Liu[3], several issues related to the asymmetric flow solutions have been addressed. It has been shown that a unique asymmetric flow solution is obtained irrespective of the size of the minimum grid spacing at the solid boundary. The asymmetry could reverse sides due to the random nature of the disturbance. It has been also shown that for the same flow conditions and same section fineness ratio, diamond-section cones with sharp edges have less flow asymmetry than those of the elliptic-section cones. Moreover, it has been shown that passive control of flow asymmetry of diamond-section cones requires fence heights that are not necessarily equal to the local section width. On the other hand, passive control of flow asymmetry of circular and elliptic-section cones require fences with heights that are, at least, equal to the local section width. Again, it was also shown that unsteady periodic asymmetric flow with vortex shedding has been predicted.

In reference 4 by Kandil, Wong and Liu, several unsteady, asymmetric vortex flows with periodic vortex shedding for circular and noncircular-section cones were presented and studied.

In the present paper, we present comparisons of asymmetric flow solutions using the thin-layer and full Navier-Stokes equations. Next, we show that the flux-vector splitting scheme produces unsteady asymmetric vortex flow with periodic vortex shedding which perfectly agrees with the previously obtained solution using the flux-difference splitting scheme[1]. Finally, passive control of asymmetric flows is studied using sharp- and round-edged, thick and thin strakes.

Formulation

Governing Equations

The conservative form of the dimensionless, unsteady, compressible, full Navier-Stokes equations in terms of time-independent, body-conformed coordinates ξ^1, ξ^2 and ξ^3 is given by

$$\frac{\partial \bar{Q}}{\partial \tau} + \frac{\partial \bar{E}_m}{\partial \xi^m} - \frac{\partial \left(\bar{E}_v\right)_s}{\partial \xi^s} = 0;\ m = 1-3,\ s = 1-3 \quad (1)$$

where

$$\xi^m = \xi^m(x_1, x_2, x_3) \quad (2)$$

$$\bar{Q} = \frac{\hat{q}}{J} = \frac{1}{J}[\rho, \rho u_1, \rho u_2, \rho u_3, \rho e]^t \quad (3)$$

$$\begin{aligned}\bar{E}_m &\equiv \text{inviscid flux}\\ &= \frac{1}{J}\left[\partial_k \xi^m \hat{E}_k\right]^t\\ &= \frac{1}{J}[\rho U_m, \rho u_1 U_m + \partial_1 \xi^m p, \rho u_2 U_m\\ &\quad + \partial_2 \xi^m p, \rho u_3 U_m + \partial_3 \xi^m p, (\rho e + p) U_m]^t\end{aligned} \quad (4)$$

$$\begin{aligned}\left(\bar{E}_v\right)_s &\equiv \text{viscous and heat–conduction flux in } \xi^s \text{ direction}\\ &= \frac{1}{J}[0, \partial_k \xi^s \tau_{k1}, \partial_k \xi^s \tau_{k2}, \partial_k \xi^s \tau_{k3},\\ &\quad \partial_k \xi^s (u_n \tau_{kn} - q_k)]^t;\quad k = 1-3,\ n = 1-3\end{aligned} \quad (5)$$

$$U_m = \partial_k \xi^m u_k \quad (6)$$

The first element of the three momentum elements of Eq. (5) is given by

$$\partial_k \xi^s \tau_{k1} \equiv \frac{M_\infty \mu}{Re}\left[\left(\partial_k \xi^s \partial_1 \xi^n - \frac{2}{3}\partial_1 \xi^s \partial_k \xi^n\right)\frac{\partial u_k}{\partial \xi^n} + \partial_k \xi^s \partial_k \xi^n \frac{\partial u_1}{\partial \xi^s}\right] \quad (7)$$

The second and third elements of the momentum elements are obtained by replacing the subscript 1, everywhere in Eq. (7), with 2 and 3, respectively. The last element of Eq. (5) is given by

$$\begin{aligned}\partial_k \xi^s (u_p \tau_{kp} - q_k) \equiv \frac{M_\infty \mu}{Re}\Big[&\left(\partial_k \xi^s \partial_p \xi^n - \frac{2}{3}\partial_p \xi^s \partial_k \xi^n\right) u_p \frac{\partial u_k}{\partial \xi^n}\\ &+ \partial_k \xi^s \partial_k \xi^n u_p \frac{\partial u_p}{\partial \xi^n}\\ &+ \frac{1}{(\gamma - 1)\,Pr}\partial_k \xi^s \frac{\partial (a^2)}{\partial \xi^n}\Big];\ p = 1-3\end{aligned} \quad (8)$$

The single thin-layer approximations of the full Navier-Stokes equations demand that we only keep the derivatives in the normal direction to the body, ξ^2, in the viscous and heat flux terms in Eqs. (1), (7) and (8). Thus, we let s = 2 for the term

$\frac{\partial(\bar{E}_v)_s}{\partial\xi^s}$ in Eq. (1) and s = 2 and n = 2 in Eqs. (7) and (8). These equations reduce to

$$\frac{\partial\bar{Q}}{\partial t}+\frac{\partial\bar{E}_m}{\partial\xi^m}-\frac{\partial(\bar{E}_v)_2}{\partial\xi^2}=0 \tag{9}$$

$$\partial_k\xi^2\tau_{k1}\equiv\frac{M_\infty\mu}{Re}\left(\psi\partial_1\xi^2+\phi\frac{\partial u_1}{\partial\xi^2}\right) \tag{10}$$

$$\partial_k\xi^2\left(u_p\tau_{kp}-q_k\right)\equiv\frac{M_\infty\mu}{Re}\left\{\psi W+\phi\left[\frac{1}{2}\frac{\partial}{\partial\xi^2}\left(u_1^2+u_2^2+u_3^2\right)+\frac{1}{(\gamma-1)Pr}\frac{\partial(a^2)}{\partial\xi^2}\right]\right\} \tag{11}$$

where

$$\phi_1=\partial_k\xi^2\partial_k\xi^2,\ \psi=\frac{1}{3}\partial_k\xi^2\frac{\partial u_k}{\partial\xi^2},\ W=\partial_p\xi^2u_p \tag{12}$$

The reference parameters for the dimensionless form of the equations are L, a_∞, L/a_∞, ρ_∞ and μ_∞ for the length, velocity, time, density and molecular viscosity, respectively. The Reynolds number is defined as $Re=\rho_\infty V_\infty L/\mu_\infty$, and the pressure, p, is related to the total energy per unit mass and density by the gas equation

$$p=(\gamma-1)\rho\left[e-\frac{1}{2}\left(u_1^2+u_2^2+u_3^2\right)\right] \tag{13}$$

The viscosity is calculated from the Sutherland law

$$\mu=T^{3/2}\left(\frac{1+C}{T+C}\right),\ C=0.4317 \tag{14}$$

and the Prandtl number P_r = 0.72.

In Eqs. (1)-(12), the indicial notation is used for convenience.

Boundary and Initial Conditions

Boundary conditions are explicitly implemented. They include inflow-outflow conditions and solid-boundary conditions. At the plane of geometric symmetry, periodic conditions are used for symmetric or asymmetric flow applications on the whole computational domain (right and left domains). At the farfield inflow boundaries freestream conditions are specified, while at the far-field outflow boundaries first-order extrapolation from the interior points is used. On the solid boundary, the no-slip and no-penetration conditions are enforced; u_1 = u_2 = u_3 = 0 and the normal pressure gradient is set equal to zero. For the temperature, the adiabatic boundary condition is enforced on the solid boundary. The initial conditions correspond to the uniform flow with u_1 = u_2 = u_3 = 0 on the solid boundary.

For the passive control applications using side strakes, double thin-layer Navier-Stokes equations are used where one thin-layer is used normal to the body and another thin-layer is used normal to the strake surface. For these applications, solid-boundary conditions are enforced on both sides of the strake.

Computational Scheme

The main computational scheme used to solve the governing equations is an implicit, upwind, flux-difference splitting, finite-volume scheme. It employs the flux-difference splitting scheme of Roe. The Jacobians matrices of the inviscid fluxes, $A_s=\frac{\partial\bar{E}_s}{\partial q}$; s = 1-3, are split into backward and forward fluxes according to the signs of the eigenvalues of the inviscid Jacobian matrices. Flux limiters are used to eliminate oscillations in the shock region. The viscous and heat-flux terms are centrally differenced. The resulting difference equation is solved using approximate factorization in the ξ^1, ξ^2 and ξ^3 directions. The resulting computer program can be used to solve for the thin-layer Navier-Stokes equations and the full Navier-Stokes equations. This code is a modified version of the CFL3D which is currently called "FTNS3D". In this code, the implicit, flux-vector splitting, finite-volume scheme, which is based on the Van-Leer scheme[5], can also be used instead of the flux-difference splitting scheme. The flux-vector splitting scheme is used to solve for the unsteady asymmetric flow application in this paper. This application is a validation solution to the solution which has been previously obtained[1] for the same application using the flux-difference splitting scheme.

Since the applications in this paper cover conical flows only, the three-dimensional scheme is used to solve for locally conical flows. This is achieved by forcing the conserved components of the flow vector field to be equal at two planes of x = 0.95 and 1.0.

Computational Applications

1. Comparison of Thin-Layer and Full Navier-Stokes Asymmetric Solutions:

This numerical test has been carried out to study the differences between asymmetric solutions using the thin-layer Navier-Stokes equations and the full Navier-Stokes equations. For this purpose, supersonic flow around a 5°–semiapex angle circular cone at 20° angle of attack is considered. The freestream Mach number and Reynolds number are 1.8 and 10^5, respectively. A grid of 161x81 points in the circumferential and normal directions is generated by using a modified Joukowski transformation with a geometric series for the grid clustering. The minimum grid spacing at the solid boundary is fixed at $\Delta\xi^2=10^{-4}$, while the maximum radius of the computational domain is kept at 21 r, where r is the radius of the circular cone at the axial station of unity.

Three cases have been computed: the first is obtained using the single thin-layer Navier-Stokes equations. The second is obtained using the one-direction full Navier-Stokes equations, where all the viscous terms in the ξ^2 direction (normal) are kept. The third is obtained using the two-direction full Navier-Stokes equations, where all the viscous terms in the ξ^2 and ξ^3 directions (normal and circumferential) are kept. Figure 1 shows the results of this test in terms of the residual error versus the number of iterations, the total-pressure-loss contours and the surface-pressure coefficient versus the meridian angle θ (θ is measured from the leeward-side plane of geometric

symmetry). The residual-error figure of the thin-layer Navier-Stokes solution shows that the asymmetric solution starts after 5,000 iterations. The error drops to machine zero (10^{-10}) in about 2,500 iterations, increases six orders of magnitude after a total of 5,000 steps and then drops again producing the asymmetric stable solution after 9,000 iterations. The residual-error figure of the one-direction full Navier-Stokes solutions drops 4.5 orders of magnitude in 2,500 steps, increases one order of magnitude after a total of 3,000 steps and then drops again producing the asymmetric stable solution. It drops to machine zero in a total number of iteration steps of 6,000. The residual-error figure of the two-direction full Navier-Stokes solution drops 4.5 orders of magnitude in 2,000 steps, increases one order of magnitude after a total of 3,000 steps and then drops to machine zero in a total of number of iteration steps of 6,000. It is clear that the full Navier-Stokes equations produce the asymmetric solution faster than the thin-layer Navier-Stokes equations.

The total-pressure-loss-contours slow that the full Navier-Stokes solutions produce thicker shear layers than those of the thin-layer solution. More contour resolution in the vortex cores is produced by the full Navier-Stokes solutions than that of the thin-layer solution. Finally, the free-shear layer on the body right-side of the full Navier-Stokes solutions is shorter than that of the thin-layer solution. However, the C_p figures of the three solutions are exactly the same.

Since the thin-layer Navier-Stokes equations are invalid for low-Reynolds number flows, we used the full Navier-Stokes equations for the same application given above but with Re = 10^4. Figure 2 shows an almost symmetric flow solution which is obtained using the two-direction Navier-Stokes equations.

2. Control of Asymmetric Flow Using Sharp-Edged Thick Strakes:

Passive control of the asymmetric flow case of Fig. 1 is considered using a sharp-edged thick strakes with length equal to 0.3 of the local radius of the circular cone section. The grid used is generated by using a hyperbolic grid generator with transfinite grid interpolation to refine the grid in the strake region. The double thin-layer Navier-Stokes equations are used for this case. The iteration histories of the residual error and lift coefficients are shown in Fig. 3. This case takes 10,000 steps to obtain a stable symmetric solution with machine zero error. The total-pressure-loss contours, the cross-flow velocity and the surface-pressure coefficient of Fig. 3 show the perfectly symmetric solution. The surface-pressure coefficient shows a jump in the pressure value at the leading edges of the strakes which correspond to θ = 90° and θ = 270°. Comparisons of the C_p of Fig. 1 and Fig. 3 show that the strakes produce higher lift in addition to their function of eliminating the flow asymmetry.

3. Unsteady Asymmetry Flow Solution Using the Flux-Vector Splitting Scheme:

This flow application has been solved previously in reference 1 using the flux-difference splitting scheme by Kandil, Wong and Liu. The governing equations used were the unsteady, compressible, thin-layer, Navier-Stokes equations. The resulting solution showed unsteady asymmetric flow with periodic vortex shedding. The computed period of shedding cycle was found as 1.4 with a shedding frequency of 4.488. This flow application case is recomputed using the flux-vector splitting scheme of Van-Leer with the thin-layer Navier-Stokes equations. This flow application is that of a 5°-semiapex angle cone at 30° angle of attack, 1.8 freestream Mach number and 10^5 freestream Reynolds number. The same grid of 161x81 with minimum spacing of $\Delta\xi^2 = 10^{-4}$ is reused here. The solution is obtained using time-accurate stepping with $\Delta t = 10^{-3}$. The logarithmic residual figure, Fig. 4 shows the time history of the solution. The first 5,000 time steps show that the residual error drops 8 orders of magnitude. During these steps the flux limiters (act as numerical dissipation) are turned-on and the solution shows symmetric steady flow. Thereafter, the flux limiters are turned-off (to minimize the artificial damping) and the residual error increases 5 orders of magnitude, then drops 6 orders of magnitude and finally increases another six orders of magnitude. Next, the solution goes through a transient response for 2,000 time steps and finally it becomes periodic. This is clearly seen after the 12,000 time steps. The solution is then monitored every 100 time steps. In Fig. 4, we show the solution for one-half the cycle of vortex shedding; from n = 13,900 to n = 14,600. It is seen that vortex shedding is obtained and by comparing the solutions of n = 13,900 and n = 14,600, which are mirror images of each other, we conclude that periodic vortex shedding is also reached. Again the period of periodic shedding is $10^{-4} \times 1{,}400 = 1.4$ corresponding to a shedding frequency of 4.488, which is exactly the same as that of the flux-difference splitting.

It is conclusive that the periodic vortex-shedding solutions are confirmed. The reason that some researchers could not obtain the periodic vortex-shedding case using the flux-vector splitting is simply because of the artificial dissipation produced by the flux limiters. This numerical dissipation produces high damping effect which suppresses the random disturbance of the solution. By turning-off the flux limiters, the random disturbance solution can grow producing the asymmetric unsteady vortex shedding flow. It should be noticed that the flux-difference splitting scheme of Roe is less dissipative than that of the flux-vector splitting scheme of Van-Leer. This is why we could obtain the unsteady vortex shedding solution of reference 1 even with the flux limiters turned-on.

4. Control of Unsteady Asymmetric Flow Using Sharp-Edged and Round-Edged Thick and Thin Strakes

Passive control of unsteady asymmetric flow case of Fig. 4 is considered using different shapes and orientations of strakes. In all the numerical tests presented in Figs. 5–8, the strake length is 0.3 of the local radius of the circular cone section. Figure 7 shows sample of typical grids which are used with the

flat-plate strakes with different orientations, δ = 0°, 10° and –10° (where δ = strakes with different orientation angle). The grid is generated by using a hyperbolic grid generator with transfinite grid interpolation to refine the grid in the strake region. The double, thin-layer Navier-Stokes equations are used in this analysis. In Fig. 5, sharp-edged thick strakes, which have the same geometry as that of Fig. 3, are used. The strakes are still effective in eliminating the unsteady asymmetric vortex-shedding flow at this high angle of attack. The resulting flow is perfectly symmetric with a lift coefficient higher than that of the unsteady asymmetric flow of Fig. 4. Again, the C_p curve of Fig. 5 shows a jump in the pressure coefficient at the strakes leading edge at θ = 90° and θ = 270°. The resulting symmetric primary vortex cores are closer to the leeward plane of symmetry and higher above the body surface than those of Fig. 3. It took 11,000 iteration steps to reach this stable symmetric solution.

In Fig. 6, we replaced the sharp-edged thick strakes with round-edged thick strakes which again produced a perfectly symmetric solution in 6,000 iteration steps. The lift coefficient is a little less than that of the sharp-edged thick strakes. The resulting symmetric primary vortex core are a little closer to the leeward plane of symmetry and a little less high above the body surface than those of Fig. 5.

In Fig. 7, we use flat-plate strakes at orientation angle δ = 0°, 10° and –10°, where δ is measured from the horizontal line at θ = 90°. All three cases produce perfectly symmetric solutions. The case with δ = –10° produces the highest lift coefficient followed by the case of δ = 0° and then the case of δ = 10°. The case of δ = –10° took 6,000 iteration steps, the case of δ = 10° took 8,000 iteration steps and the case of δ = 0° took 10,000 iteration steps, all to reach a stable symmetric solution.

Concluding Remarks

In this paper, the unsteady, compressible, thin-layer and Navier-Stokes equations are used to study several aspects of asymmetric vortex flow around circular cones and its passive control. The main computational scheme which is used to produce the steady flow results is the implicit, upwind, flux-difference splitting, finite-volume scheme. Comparisons of the thin-layer and full Navier-Stokes asymmetric solutions show that the full Navier-Stokes equations produce thicker shear-layers than those produced by the thin-layer equations. Moreover, the full Navier-Stokes equations give better resolution in the vortex cores. Finally, the full Navier-Stokes equations produce the asymmetric flows faster than the thin-layer equations. It has also been shown that the flux-vector splitting scheme without flux limiters produces the same unsteady asymmetric flow with periodic vortex shedding as that of the flux-difference splitting scheme with flux limiters. Finally, passive control of steady and unsteady asymmetric flow has been demonstrated by using several shapes of strakes. While the strakes eliminate the flow asymmetry, they produce high lift for the configuration.

Acknowledgements

The research work has been supported by the NASA Langley Research Center under grants No. NAS-1–18584–71 and NAG-1–994.

References

1. Kandil, O. A., Wong, T-C. and Liu, C. H., "Prediction of Steady and Unsteady Asymmetric Vortical Flow Around Cones," AIAA 90–0598, January 1990.
2. Siclari, M. J., "Asymmetric Separated Flows at Supersonic Speeds," AIAA 90–0595, January 1990.
3. Kandil, O. A., Wong, T-C. and Liu, C. H., "Asymmetric Flow Around Cones with Noncircular Sections," AGARD Symposium on Missile Aerodynamics, Paper No. 16, Friedrichshafen, FRG, April 1990.
4. Kandil, O. A., Wong, T-C. and Liu, C. H., "Numerical Simulation of Steady and Unsteady Asymmetric Vortical Flows," ASME Symposium on Non-Steady Fluid Dynamics, Toronto, Canada, June 1990.
5. Rumsey, L. C. and Anderson, W. Kyle, "Some Numerical Aspects of Unsteady Navier-Stokes Computations of Unsteady Navier-Stokes Computations over Airfoils Using Dynamic Meshes," AIAA 88–0329, January 1988.

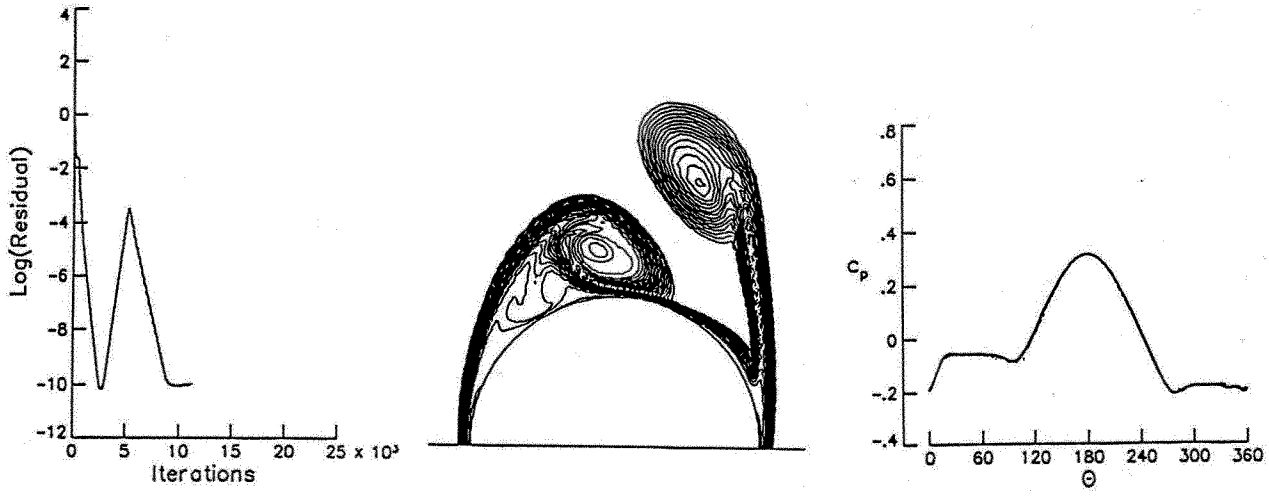

Thin-Layer Navier-Stokes Solution

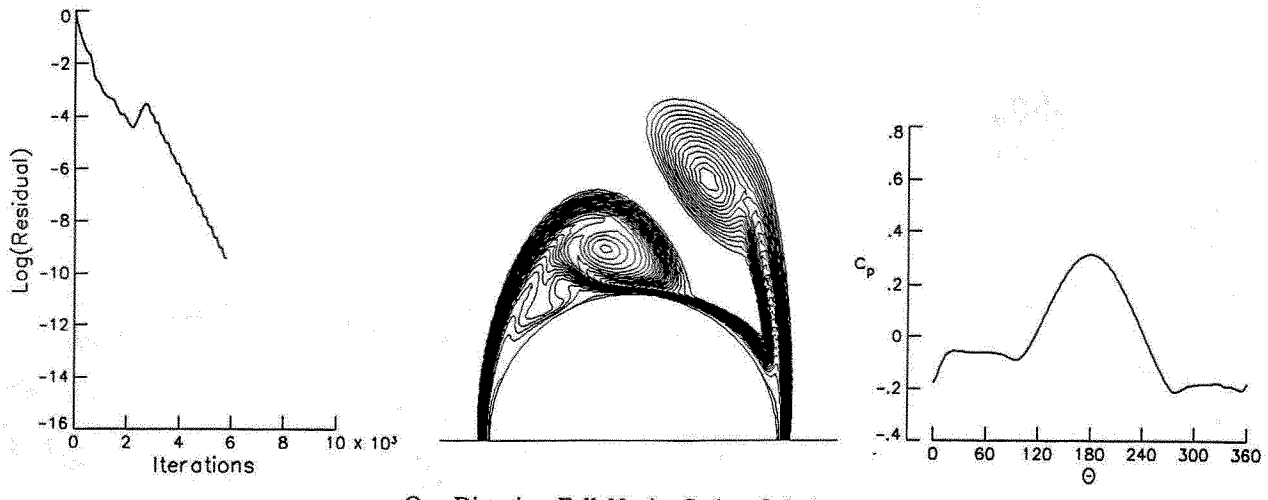

One-Direction Full Navier-Stokes Solution

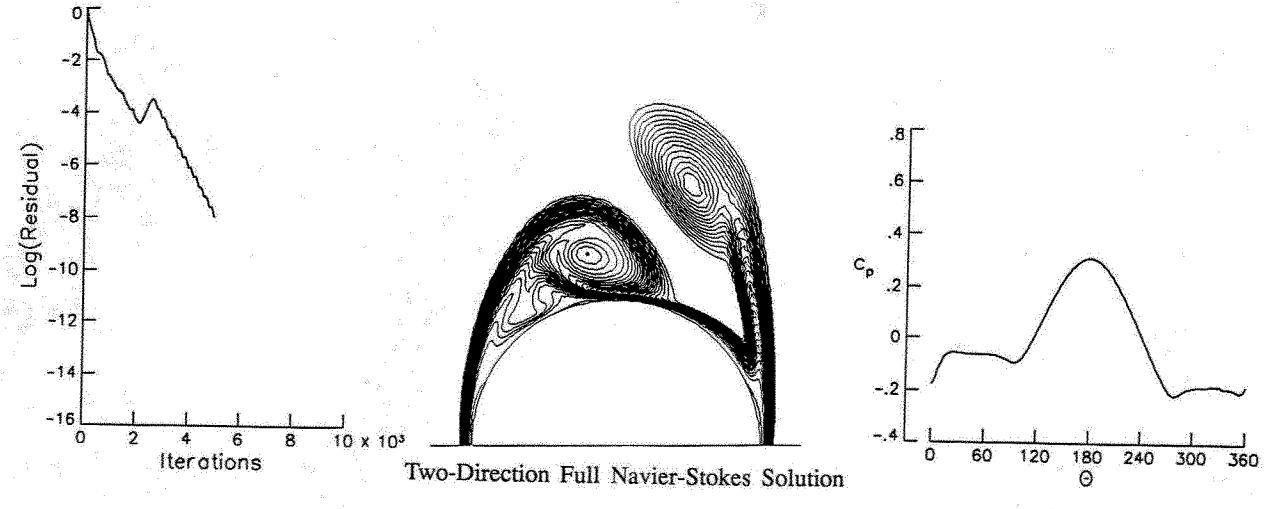

Two-Direction Full Navier-Stokes Solution

Fig. 1. Comparison of thin-layer and Full-Navier-Stokes asymmetric solutions for a circular cone; α = 20 deg, M_∞ = 1.8, $R_e = 10^5$.

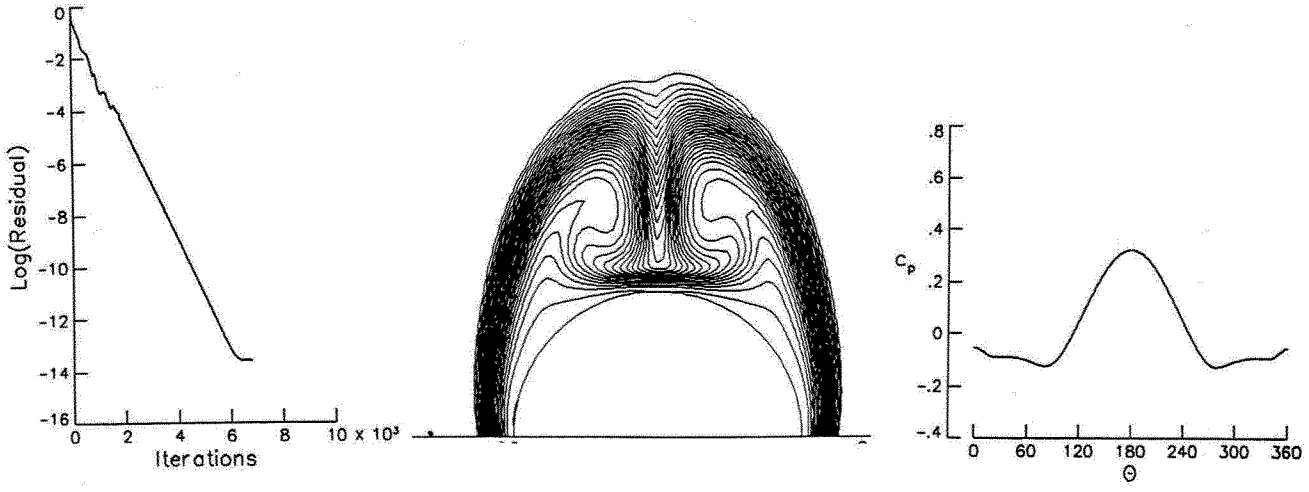

Fig. 2. Full Navier-Stokes symmetric solution for a circular cone; α = 20 deg, M_∞ = 1.8, R_e = 10^4.

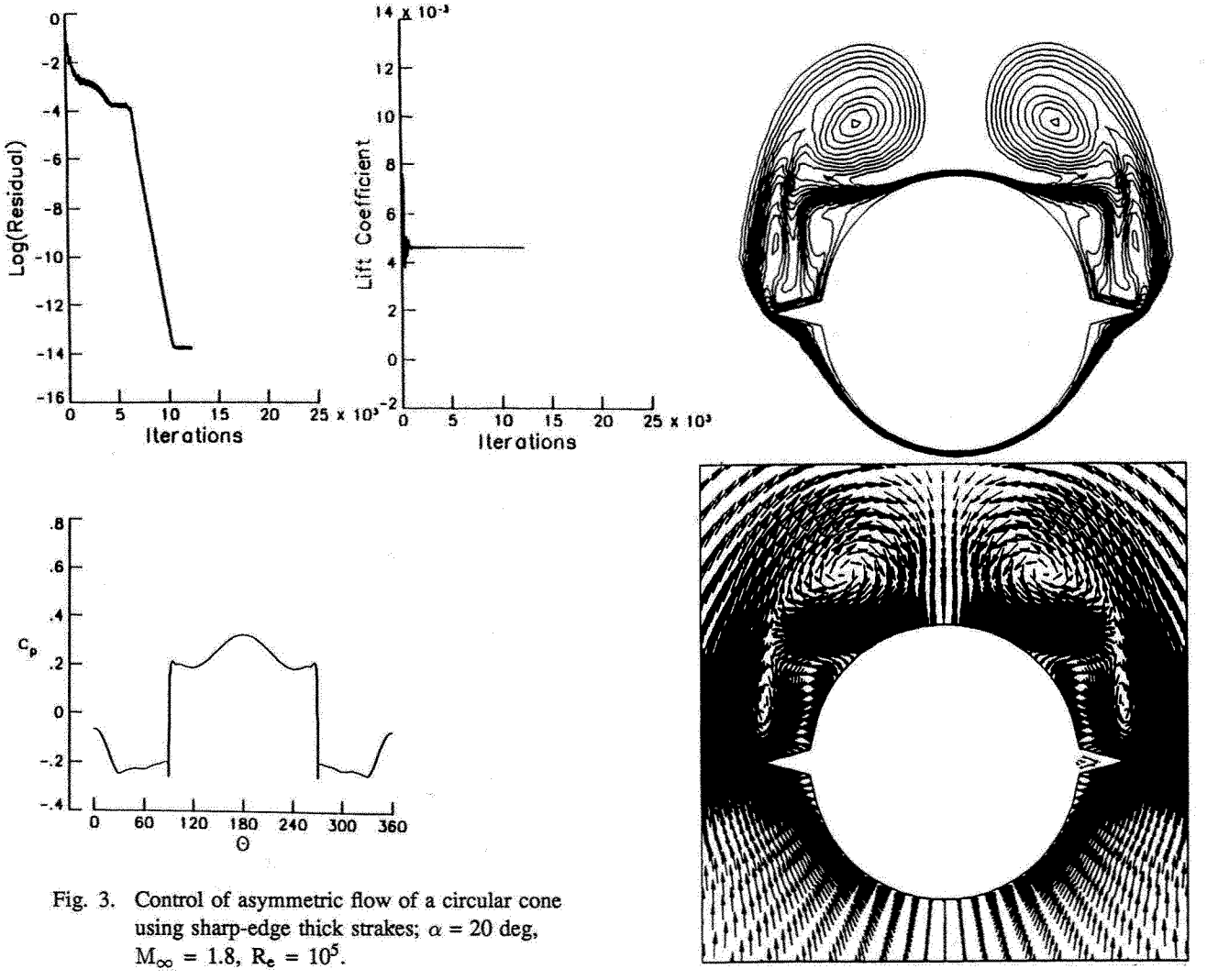

Fig. 3. Control of asymmetric flow of a circular cone using sharp-edge thick strakes; α = 20 deg, M_∞ = 1.8, R_e = 10^5.

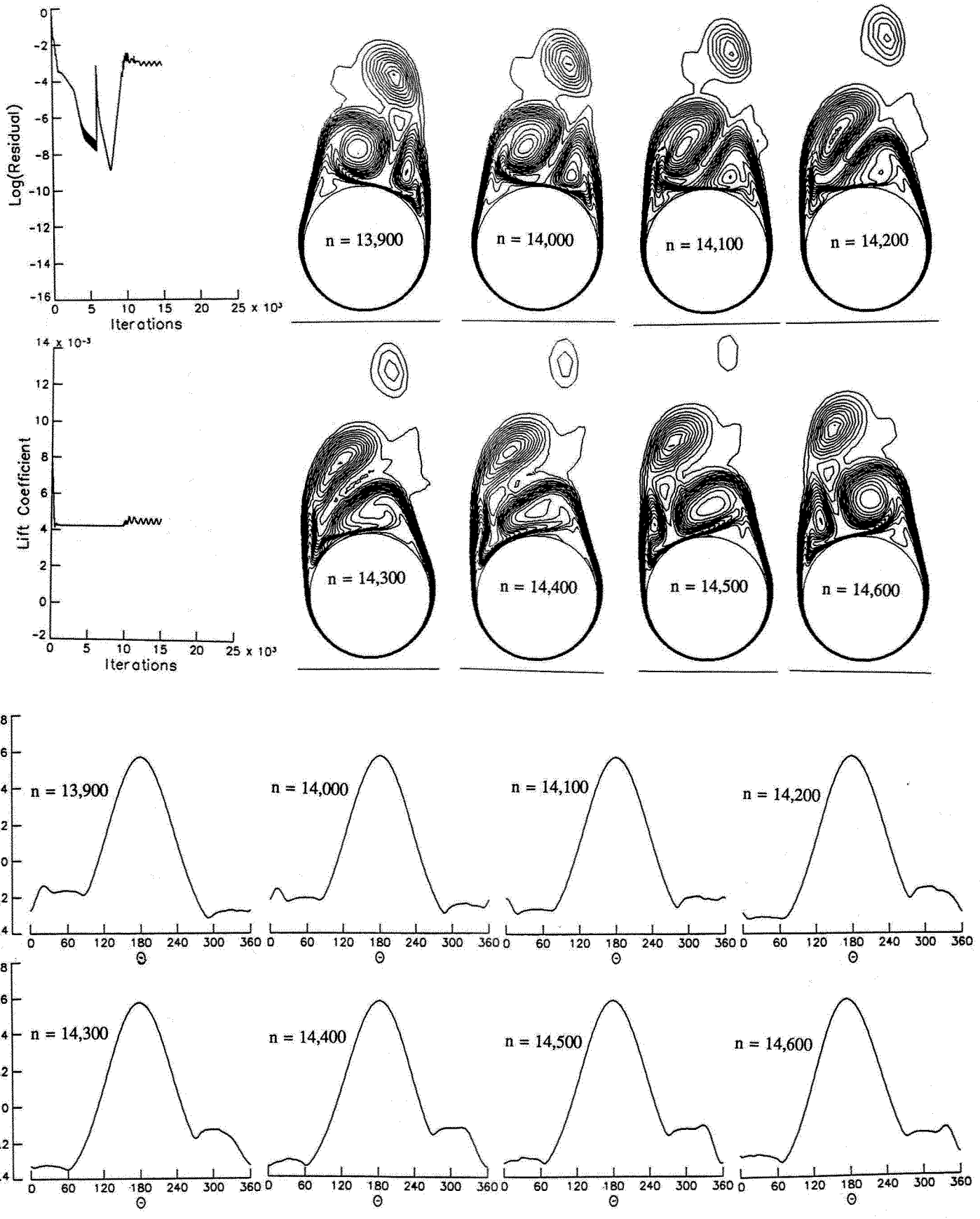

Fig. 4. Unsteady asymmetric flow solution (using flux-vector splitting) with vortex shedding for a circular cone during periodic flow responses; α = 30 deg, M_∞ = 1.8, $R_e = 10^5$, $\Delta t = 10^{-3}$.

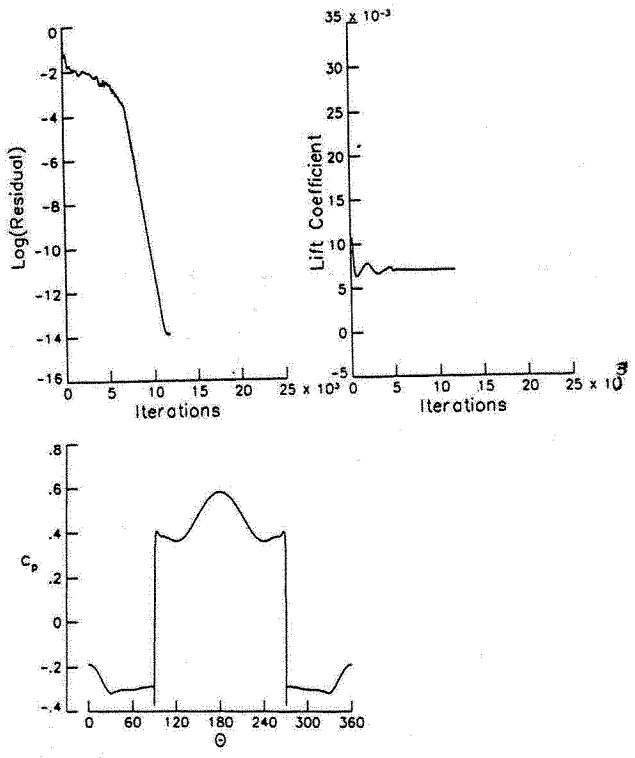

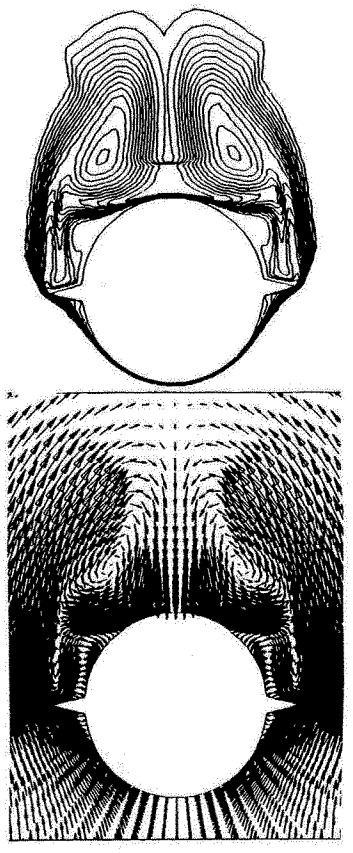

Fig. 5. Control of asymmetric flow of a circular cone using sharp-edged thick strakes; $\alpha = 30°$, $M_\infty = 1.8$, $R_e = 10^5$.

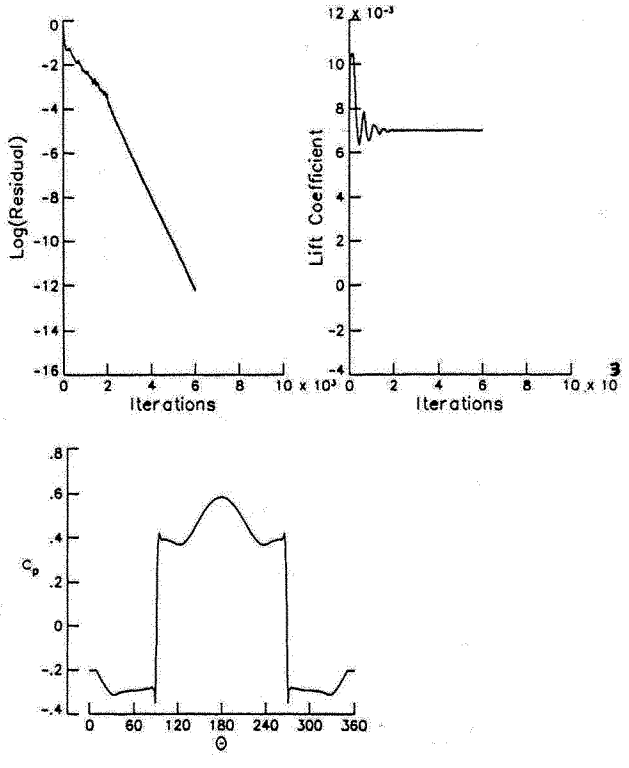

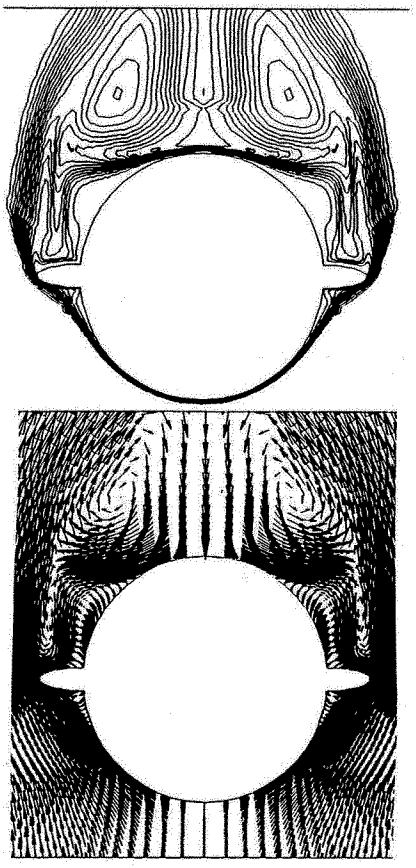

Fig. 6. Control of asymmetric flow of a circular cone using round-edged thick strakes, $\alpha = 30$ deg, $M_\infty = 1.8$, $R_e = 10^5$.

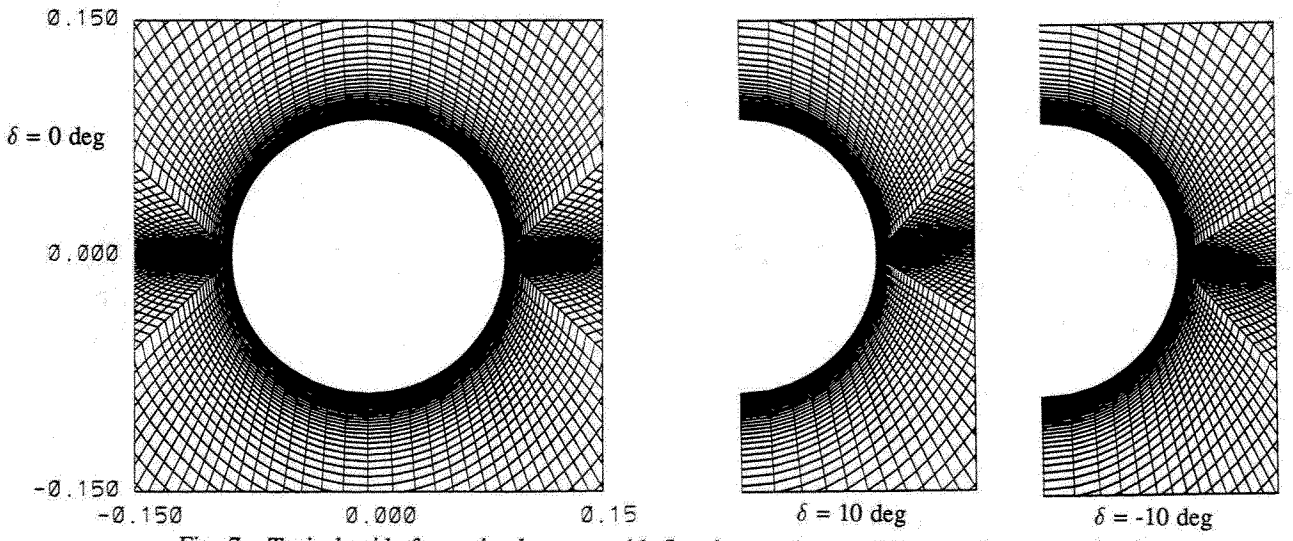

Fig. 7. Typical grids for a circular-cone with flat-plate strakes of different orientations δ = 0 deg, 10 deg and –10 deg.

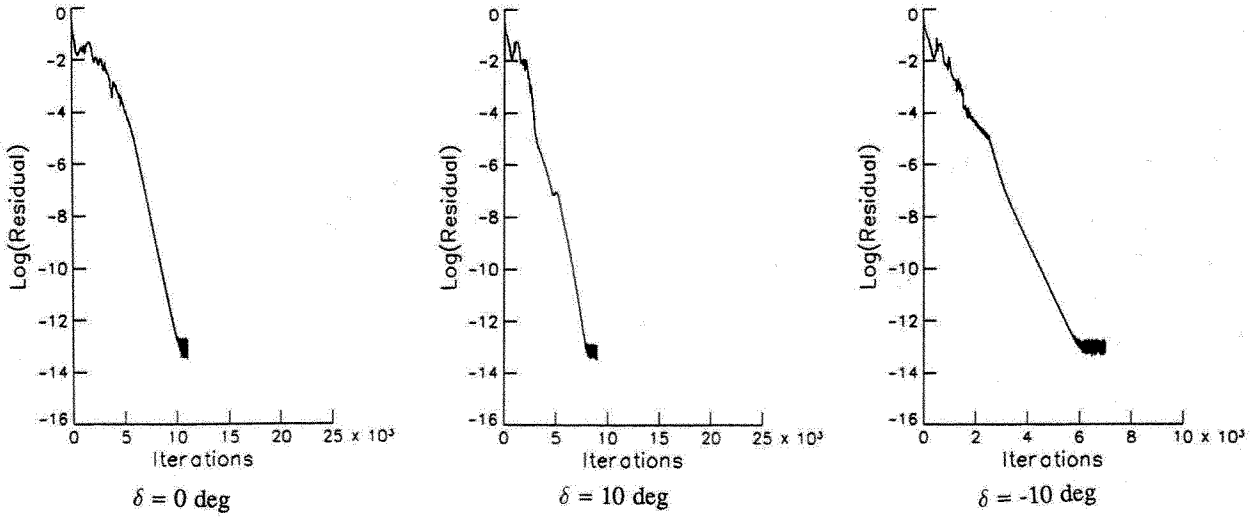

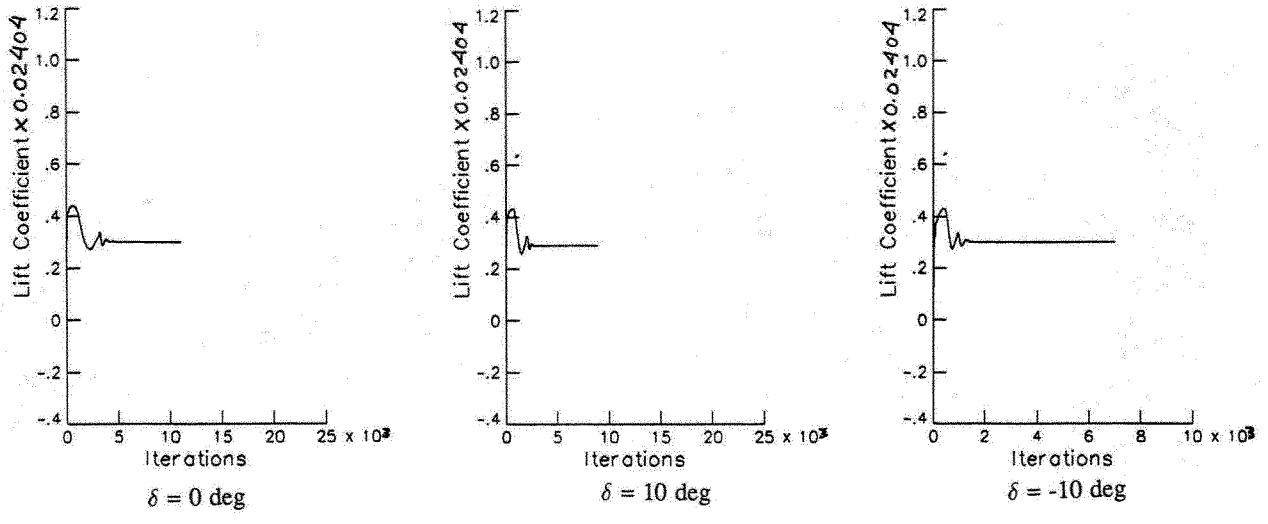

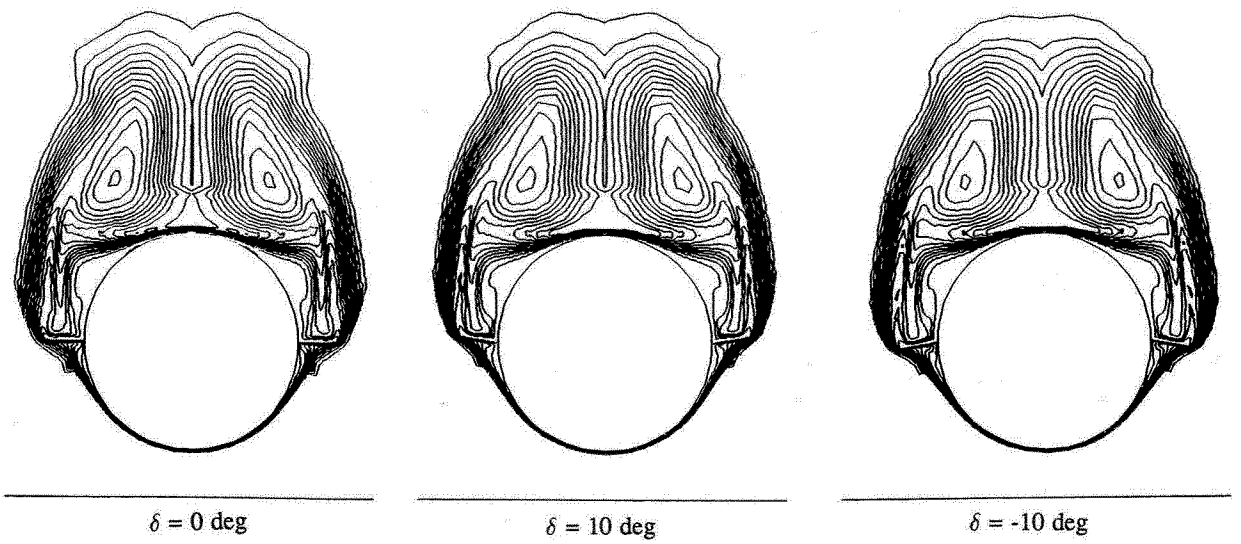

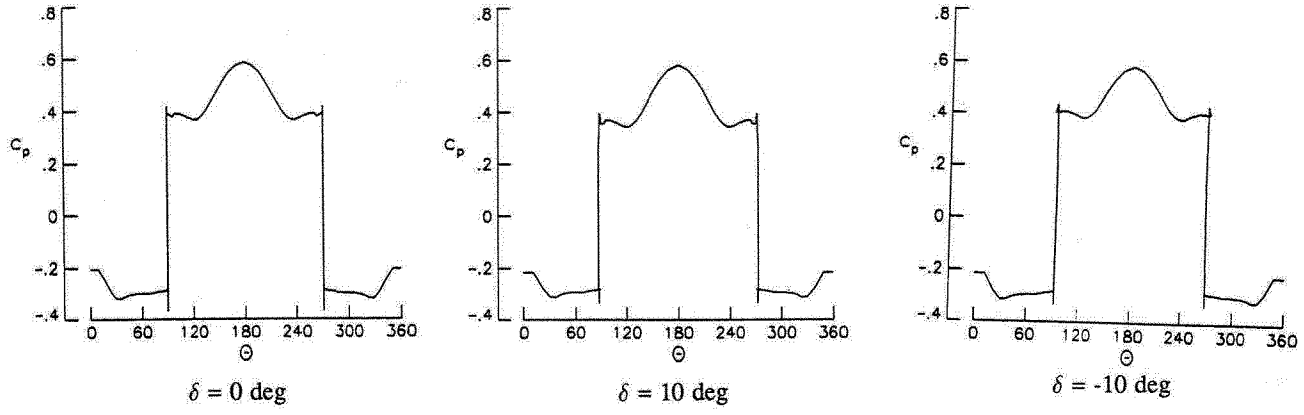

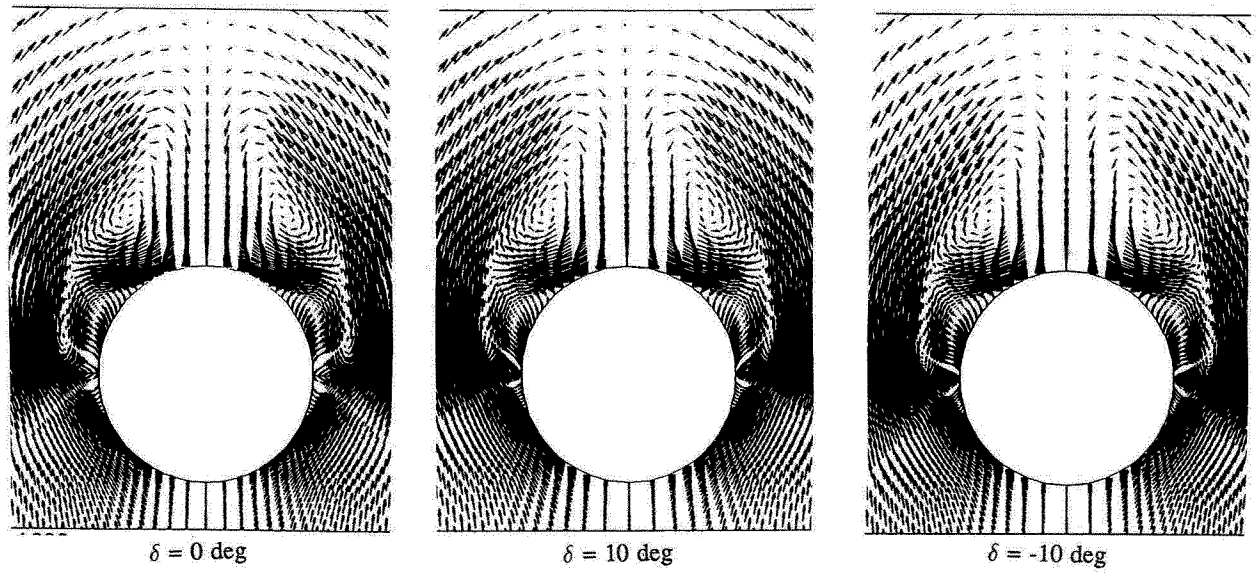

Fig. 8. Control of asymmetric flow of a circular cone using flat plate strakes of different orientations δ = 0 deg, 10 deg and –10 deg; α = 30 deg, M_∞ = 1.8, $R_e = 10^5$